



**HAL**  
open science

# An unfitted Nitsche method for incompressible fluid-structure interaction using overlapping meshes

Erik Burman, Miguel Angel Fernández

► **To cite this version:**

Erik Burman, Miguel Angel Fernández. An unfitted Nitsche method for incompressible fluid-structure interaction using overlapping meshes. [Research Report] RR-8424, 2013. hal-00918272v1

**HAL Id: hal-00918272**

**<https://inria.hal.science/hal-00918272v1>**

Submitted on 13 Dec 2013 (v1), last revised 28 Apr 2014 (v3)

**HAL** is a multi-disciplinary open access archive for the deposit and dissemination of scientific research documents, whether they are published or not. The documents may come from teaching and research institutions in France or abroad, or from public or private research centers.

L'archive ouverte pluridisciplinaire **HAL**, est destinée au dépôt et à la diffusion de documents scientifiques de niveau recherche, publiés ou non, émanant des établissements d'enseignement et de recherche français ou étrangers, des laboratoires publics ou privés.



# An unfitted Nitsche method for incompressible fluid-structure interaction using overlapping meshes

Erik Burman, Miguel A. Fernández

**RESEARCH  
REPORT**

**N° 8424**

December 2013

Project-Team Reo





## An unfitted Nitsche method for incompressible fluid-structure interaction using overlapping meshes

Erik Burman\*, Miguel A. Fernández<sup>†‡</sup>

Project-Team Reo

Research Report n° 8424 — December 2013 — 24 pages

**Abstract:** We consider the extension of the Nitsche method to the case of fluid-structure interaction problems on unfitted meshes. We give a stability analysis for the space semi-discretized problem and show how this estimate may be used to derive optimal error estimates for smooth solutions, irrespectively of the mesh/interface intersection. We also discuss different strategies for the time discretization, using either fully implicit or explicit coupling (*loosely coupled*) schemes. Some numerical examples illustrate the theoretical discussion.

**Key-words:** fluid-structure interaction, incompressible fluid, unfitted meshes, fictitious domain method, Nitsche method, coupling schemes.

---

The first author received funding for this research from EPSRC (award number EP/J002313/1). The second author was financially supported by the French National Research Agency (ANR) through the EXIFSI project (ANR-12-JS01-0004).

\* Department of Mathematics, University College London, London, UK-WC1E 6BT, United Kingdom

† Inria, REO project-team, Rocquencourt - B.P. 105, F-78153 Le Chesnay cedex, France

‡ UPMC Université Paris VI, REO project-team, UMR 7958 LJLL, F-75005 Paris, France

**RESEARCH CENTRE  
PARIS – ROCQUENCOURT**

Domaine de Voluceau, - Rocquencourt  
B.P. 105 - 78153 Le Chesnay Cedex

## Une méthode Nitsche en interaction fluide-structure avec des maillages non compatibles

**Résumé :** Nous considérons l'extension de la méthode Nitsche au cas des problèmes d'interaction fluide-structure avec des maillages non compatibles. Nous analysons la stabilité du problème semi-discrétisé en espace et montrons comment cette estimation peut être utilisée pour obtenir des estimations d'erreur optimales pour des solutions régulières, indépendamment de l'intersection maillage/interface. Nous présentons également différentes stratégies de discrétisation en temps, basées dans des schémas de couplage totalement implicites ou explicites (*faiblement couplés*). Quelques exemples numériques illustrent la discussion théorique.

**Mots-clés :** interaction fluide-structure, fluide incompressible, maillages non compatibles, méthode de domaine fictif, méthode de Nitsche, schémas de couplage.

## 1 Introduction

The use of Nitsche’s method for the coupling of multiphysics problems in computational mechanics has received increasing attention recently [20]. Thanks to the flexibility and the mathematical soundness of the Nitsche method it has been used to design methods for several problems of computational mechanics. Examples include XFEM of elasticity, i.e. interface problems on unfitted meshes [17, 18], and robust and accurate fictitious domain methods [9]. Nitsche’s method was first applied to fluid-structure interaction problems in the framework of space-time Galerkin methods in [21] and used to design stable loosely coupled fluid-structure interaction methods in [6, 7]. The objective of this note is to apply these techniques to design a computational method for fluid-structure interaction on unfitted meshes. The use of fictitious domain or immersed boundary methods for the numerical modelisation of fluid-structure interaction problems was pioneered in the works [16] and [1, 11] and has recently seen a surge of interest in papers such as [24, 15, 3]. Our contribution in the present paper is to show how Nitsche’s method can be used for fluid-structure computations on unfitted meshes. We present a rigorous proof that optimal convergence in energy norm is obtained for smooth solutions in the space semi-discretized case. Then we discuss different strategies for the time discretization, either fully implicitly or the explicit coupling (or *loosely coupled*) schemes introduced in [6, 7].

We will study the case where the solid body is meshed, hence on the solid side the mesh is fitted to the interface. This solid mesh is then glued onto the fluid domain without respecting the mesh on the fluid side. This approach is similar to that proposed in [19] for the Poisson problem and more recently in [25] for the Stokes’ equations. The heterogeneous character of the present system however leads to some difficulties compared to these works. The Nitsche method uses explicit integration of normal stress on the interface to ensure consistency, since the stress is continuous the stress may be taken from either the solid or the fluid system. Indeed in [19], robustness is ensured by taking all the stresses on the side where the mesh is conforming. This choice is convenient in the homogeneous case, but appears not to be so appealing in the case of fluid structure interaction. The reason for this is that there is no dissipative mechanism in the solid elastodynamic system that can absorb the perturbation induced by the boundary stresses on the solid side. If on the other hand the Nitsche mortaring is taken only from the fluid side as proposed in [21], the trace inequality necessary for the analysis is no longer robust and the penalty parameter may have to be chosen very large for unfortunate cuts of the mesh, or the resulting system matrix may turn out to be singular. In order to nevertheless design a robust and accurate method we suggest to use a ghost penalty term in the fluid (See [5] or [8] where this technique was proposed for fictitious domain methods for Stokes’ problem) in order to extend the coercivity to all of the mesh domain  $\Omega_{\mathcal{T}}$  consisting of all triangles with non-zero intersection with  $\Omega$ . This is a weakly consistent stabilization term that extends the  $H^1$ -stability of the viscous dissipation, as well as the control of the fluid pressure, to the whole fluid mesh-domain, i.e. also to parts of cut elements that are outside the physical domain. We prove in this note that this is sufficient for the method to be stable and optimally convergent. The extended stability is necessary both for the velocities and the pressures. In addition the solid system must be shown to satisfy a special patch test, in the form of an interpolation operator with certain orthogonality properties on the interface, in order to decouple from the fluid system in the analysis. It is worthwhile to observe that the present analysis also applies without modifications to the case where both meshes are fitted to the interface (but not necessarily conforming) and to the best of our knowledge it is the first analysis of that case as well.

Note that the mass-matrices may be poorly conditioned if some nodes have macroelements with very small intersection with the physical domain. The space discretization operator of the fluid system however will have a condition number that is uniform in the mesh-interface

intersection (see [25] for a proof) and it is known that the poor conditioning of the mass-matrix can be alleviated by diagonal scaling.

An outline of the paper is as follows. In Section 2 we present a model problem for fluid-structure interaction and the associated variational formulation. A fictitious domain fluid-structure interaction discretization of the weak formulation is formulation and the different interface terms discussed. This scheme is then analyzed in Section 3.3. Stability and optimal convergence for smooth solutions is proven for the space-semi discretized system. Finally in Section 5 we show some numerical examples where we compare the performance of the fitted and the unfitted methods on some two-dimensional model problems. Section 6 is dedicated to some concluding remarks.

## 2 A linear model problem

We consider a low Reynolds regime and assume that the structure undergoes infinitesimal displacements. The computational domain consists of  $\Omega \stackrel{\text{def}}{=} \Omega^f \cup \Omega^s \cup \Sigma$  with  $\Omega^f$ ,  $\Omega^s$  the fluid and solid subdomain, respectively, and  $\Sigma \stackrel{\text{def}}{=} \overline{\Omega^f} \cap \overline{\Omega^s}$  the fluid-solid interface. The exterior unit-vector normal to  $\partial\Omega$  is denoted by  $\mathbf{n}$ . We consider a partition  $\partial\Omega^f = \Gamma^d \cup \Gamma^n \cup \Sigma$  of the fluid boundary, where  $\Sigma$  stands for the fluid-structure interface, with unit normal  $\mathbf{n}_\Sigma$  pointing into  $\Omega^s$ . The fluid is described by the Stokes equations in a polyhedral domain  $\Omega^f$  and the structure by the elastodynamics equations in  $\Omega^s$ . The considered coupled problem reads therefore as follows: find the fluid velocity  $\mathbf{u} : \Omega^f \times \mathbb{R}^+ \rightarrow \mathbb{R}^d$ , the fluid pressure  $p : \Omega^f \times \mathbb{R}^+ \rightarrow \mathbb{R}$ , the solid displacement  $\mathbf{d} : \Omega^s \times \mathbb{R}^+ \rightarrow \mathbb{R}^d$  and the solid velocity  $\dot{\mathbf{d}} : \Omega^s \times \mathbb{R}^+ \rightarrow \mathbb{R}^d$  such that

$$\begin{cases} \rho^f \partial_t \mathbf{u} - \mathbf{div} \boldsymbol{\sigma}^f(\mathbf{u}, p) = \mathbf{0} & \text{in } \Omega, \\ \mathbf{div} \mathbf{u} = 0 & \text{in } \Omega, \\ \mathbf{u} = \mathbf{0} & \text{on } \Gamma^d, \\ \boldsymbol{\sigma}(\mathbf{u}, p) \mathbf{n} = \mathbf{0} & \text{on } \Gamma^n, \end{cases} \quad (1)$$

$$\begin{cases} \dot{\mathbf{d}} = \partial_t \mathbf{d} & \text{in } \Omega^s, \\ \rho^s \partial_t \dot{\mathbf{d}} - \mathbf{div} \boldsymbol{\sigma}^s(\mathbf{d}) = \mathbf{0} & \text{in } \Omega^s, \\ \mathbf{d} = \mathbf{0} & \text{on } \Gamma^d, \\ \boldsymbol{\sigma}(\mathbf{d}) \mathbf{n} = \mathbf{0} & \text{on } \Gamma^n \end{cases} \quad (2)$$

$$\begin{cases} \mathbf{u} = \dot{\mathbf{d}} & \text{on } \Sigma, \\ \boldsymbol{\sigma}^f(\mathbf{u}, p) \mathbf{n}_\Sigma = \boldsymbol{\sigma}^s(\mathbf{d}) \mathbf{n}_\Sigma & \text{on } \Sigma \end{cases} \quad (3)$$

and complemented with the initial conditions  $\mathbf{u}(0) = \mathbf{u}^0$ ,  $\mathbf{d}(0) = \mathbf{d}^0$ ,  $\dot{\mathbf{d}}(0) = \dot{\mathbf{d}}^0$ . Here,  $\rho^f$  and  $\rho^s$  respectively denote the fluid and solid densities, and  $\boldsymbol{\sigma}^s(\mathbf{d})$  the solid stress-tensor. The fluid Cauchy-stress tensor is given by

$$\boldsymbol{\sigma}^f(\mathbf{u}, p) \stackrel{\text{def}}{=} -p \mathbf{I} + 2\mu \boldsymbol{\epsilon}(\mathbf{u}), \quad \boldsymbol{\epsilon}(\mathbf{u}) \stackrel{\text{def}}{=} \frac{1}{2} (\nabla \mathbf{u} + \nabla \mathbf{u}^T)$$

where  $\mu$  stands for the fluid dynamic viscosity and  $\mathbf{I}$  the identity matrix in  $\mathbb{R}^d$ .

Though simplified, problem (1)-(2) features some of the main numerical issues that appear in complex non-linear fluid-structure interaction problems involving an incompressible fluid (see, e.g., [10, 13]). Well-posedness results for this type of linear fluid-structure interaction problems can be found in [12] (see also [23]).

In what follows, we will consider the usual Sobolev spaces  $H^m(\omega)$  ( $m \geq 0$ ), with norm  $\|\cdot\|_{m,\omega}$ . The closed subspaces  $H_0^1(\omega)$ , consisting of functions in  $H^1(\omega)$  with zero trace on  $\partial\omega$ , and  $L_0^2(\omega)$ , consisting of function in  $L^2(\omega)$  with zero mean in  $\omega$ , will also be used. The scalar product in  $L^2(\omega)$  is denoted by  $(\cdot, \cdot)_\omega$  and its norm by  $\|\cdot\|_{0,\omega}$ . In order to ease the notation, we set  $(\cdot, \cdot) \stackrel{\text{def}}{=} (\cdot, \cdot)_\Omega$ .

For the weak formulation of the solid we introduce the abstract bi-linear form  $a^e : \mathbf{W} \times \mathbf{W} \rightarrow \mathbb{R}$  describing the elastic behavior of the structure, where  $\mathbf{W}$  stands for its space of admissible displacements.

We assume that  $a^e$  is an inner-product into  $\mathbf{W} \subset [H_0^1(\Omega^s)]^d$  and that, endowed with this inner-product,  $\mathbf{W}$  is a Hilbert space. We set

$$\|\mathbf{w}\|_e \stackrel{\text{def}}{=} a^e(\mathbf{w}, \mathbf{w})^{\frac{1}{2}}$$

and we assume that the following continuity estimate holds

$$\|\mathbf{w}\|_e^2 \leq \beta^e \|\mathbf{w}\|_{1,\Omega^s}^2 \quad (4)$$

for all  $\mathbf{w} \in \mathbf{W}$ .

We also introduce the fluid velocity and pressure functional spaces

$$\mathbf{V} \stackrel{\text{def}}{=} \{\mathbf{v} \in [H^1(\Omega^f)]^d / \mathbf{v}|_{\Gamma^d} = \mathbf{0}\}, \quad Q \stackrel{\text{def}}{=} L^2(\Omega),$$

equipped with the norms  $\|\mathbf{v}\|_{\mathbf{V}} \stackrel{\text{def}}{=} \|\mu^{\frac{1}{2}} \nabla \mathbf{v}\|_{0,\Omega}$ ,  $\|q\|_Q = \|\mu^{-\frac{1}{2}} q\|_{0,\Omega}$ . Finally, the standard bi-linear forms for the Stokes problem,  $a : \mathbf{V} \times \mathbf{V} \rightarrow \mathbb{R}$  and  $b : Q \times \mathbf{V} \rightarrow \mathbb{R}$ , given by

$$a(\mathbf{u}, \mathbf{v}) \stackrel{\text{def}}{=} 2\mu(\boldsymbol{\epsilon}(\mathbf{u}), \boldsymbol{\epsilon}(\mathbf{v})), \quad b(q, \mathbf{v}) \stackrel{\text{def}}{=} -(q, \text{div} \mathbf{v}),$$

will be used.

### 3 Space semi-discretization: Nitsche fictitious domain formulation

Let  $\{\mathcal{T}_h\}_{0 < h \leq 1}$  denote a family of triangulations of  $\Omega^s \cup \Omega^f$ . The mesh on  $\Omega^s$  is fitted to the interface,  $\mathcal{T}_h^s \equiv \bar{\Omega}^s$  whereas that of  $\Omega^f$  is not  $\Omega^f \subset \mathcal{T}_h^f$ ,  $\Omega^f \not\equiv \mathcal{T}_h^f$ . We will denote by  $\Omega_{\mathcal{T}^f}$  the set of  $\mathbb{R}^d$  coinciding with  $\mathcal{T}_h^f$  (see Figure 1). For each triangulation  $\mathcal{T}_h$ , the subscript  $h \in (0, 1]$

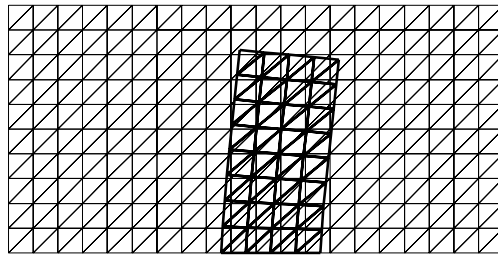


Figure 1: Example of overlapping fluid-solid meshes.

refers to the level of refinement of the triangulation, which is defined by  $h \stackrel{\text{def}}{=} \max_{K \in \mathcal{T}_h} h_K$ ,

with  $h_K$  the diameter of  $K$ . In order to simplify the presentation, we assume that the family of triangulations is quasi-uniform. We assume that the element faces in the solid trace mesh on  $\Sigma$  are grouped in macropatches  $F_i$  with  $\text{meas}(F_i) = O(h)$  and each  $F_i$  containing at least one (d-1) dimensional macro patch containing an interior node. We will use the following discrete semi-norms on function values on the trace  $\Sigma$ ,

$$\|u\|_{\pm\frac{1}{2},h,\Sigma} \stackrel{\text{def}}{=} \left( \int_{\Sigma} h^{\mp 1} u^2 \, ds \right)^{\frac{1}{2}}.$$

We also note that the following trace inequality holds for all functions in  $H^1(K)$ , there exists  $C_T > 0$  such that for all line segments  $\Sigma$  intersecting  $K$  there holds

$$\|u\|_{0,K \cap \Sigma} \leq C_T (h^{-\frac{1}{2}} \|u\|_{0,K} + h^{\frac{1}{2}} \|\nabla u\|_{0,K}). \quad (5)$$

For shape regular elements, the proof of this result is equivalent to that of the standard trace inequality. In what follows, we let  $X_h$  denote the standard space of continuous piecewise affine functions:

$$X_h \stackrel{\text{def}}{=} \{v_h \in C^0(\bar{\Omega}) / v_h|_K \in \mathbb{P}_1(K) \quad \forall K \in \mathcal{T}_h\}. \quad (6)$$

For the approximation of the fluid velocity we will consider the space  $\mathbf{V}_h \stackrel{\text{def}}{=} [X_h]^d \cap \mathbf{V}$  and for the pressure we will use either  $Q_h \stackrel{\text{def}}{=} X_h \cap Q$ . We assume that the pressure stabilization operator,  $s_p : Q_h \times Q_h \rightarrow \mathbb{R}$ , satisfies

$$c_1 \|h \nabla p_h\|_{0,\Omega_f^f}^2 \leq s_p(p_h, p_h) \leq c_2 \|h \nabla p_h\|_{0,\Omega_f^f}^2.$$

For instance the classical Brezzi-Pitkäranta pressure stabilization [4] may be used on the following form

$$s_h(p_h, q_h) \stackrel{\text{def}}{=} \int_{\Omega_f^f} \frac{h^2}{\mu} \nabla p_h \cdot \nabla q_h \, dx. \quad (7)$$

We also assume that the velocity stabilization operator,  $g_h : V_h \times V_h \rightarrow \mathbb{R}$ , is designed so that the following stability holds (see [5] for examples of suitable operators and a proof).

**Lemma 1** *For all  $\mathbf{v}_h \in V_h$  there holds*

$$c_s (\mu \|\boldsymbol{\epsilon}(\mathbf{v}_h)\|_{0,\Omega_{\mathcal{T}_h}}^2 + g_h(\mathbf{v}_h, \mathbf{v}_h)) \leq \mu \|\boldsymbol{\epsilon}(\mathbf{v}_h)\|_{0,\Omega}^2 + g_h(\mathbf{v}_h, \mathbf{v}_h). \quad (8)$$

*Note that the velocity stabilization only is needed in the interface zone and can in principle be localized to elements  $K$  for which the constant of the trace inequality controlling the boundary trace by the norm on  $\Omega^f \cap K$  is very large.*

We denote the total fluid stabilization by

$$S_h((\mathbf{u}_h, p_h), (\mathbf{v}_h, q_h)) \stackrel{\text{def}}{=} s_h(p_h, q_h) + g_h(\mathbf{u}_h, \mathbf{v}_h). \quad (9)$$

Our space semi-discrete approximation of (1)-(3) reads as follows: for  $t > 0$ , find

$$(\mathbf{u}_h(t), p_h(t), \dot{\mathbf{d}}_h(t), \mathbf{d}_h(t)) \in \mathbf{V}_h \times Q_h \times \mathbf{W}_h \times \mathbf{W}_h,$$

such that  $\dot{\mathbf{d}}_h(t) = \partial_t \mathbf{d}_h(t)$  and

$$\begin{cases} \rho^f (\partial_t \mathbf{u}_h, \mathbf{v}_h) + A((\mathbf{u}_h, p_h), (\mathbf{v}_h, q_h)) + \rho^s (\partial_t \dot{\mathbf{d}}_h, \mathbf{w}_h)_{\Omega^s} + a^e(\mathbf{d}_h, \mathbf{w}_h) \\ \quad - (\boldsymbol{\sigma}(\mathbf{u}_h, p_h) \mathbf{n}, (\mathbf{v}_h - \mathbf{w}_h))_{\Sigma} - ((\mathbf{u}_h - \dot{\mathbf{d}}_h), \boldsymbol{\sigma}(\mathbf{v}_h, -q_h) \mathbf{n})_{\Sigma} \\ \quad + \frac{\gamma \mu}{h} ((\mathbf{u}_h - \dot{\mathbf{d}}_h), (\mathbf{v}_h - \mathbf{w}_h))_{\Sigma} + S_h((\mathbf{u}_h, p_h), (\mathbf{v}_h, q_h)) = 0. \end{cases} \quad (10)$$

for all  $(\mathbf{v}_h, q_h, \mathbf{w}_h) \in \mathbf{V}_h \times Q_h \times \mathbf{W}_h$  and where

$$A((\mathbf{u}_h, p_h), (\mathbf{v}_h, q_h)) \stackrel{\text{def}}{=} a(\mathbf{u}_h, \mathbf{v}_h) + b(p_h, \mathbf{v}_h) - b(q_h, \mathbf{u}_h).$$

### 3.1 Stability properties of the discrete scheme.

First we state a Lemma giving the coercivity on  $\Omega_T^f$  of the discretization of Stokes' system.

**Lemma 2** For  $\gamma > C_T^2$ , there exists  $c_s > 0$  such that

$$\begin{aligned} c_s \left( \mu_f \|\nabla \mathbf{u}_h\|_{0, \Omega_T^f}^2 + \gamma \mu \|\mathbf{u}_h - \dot{\mathbf{d}}_h\|_{\frac{1}{2}, h, \Sigma}^2 + |(\mathbf{u}_h, p_h)|_S^2 \right) \\ \leq A((\mathbf{u}_h, p_h), (\mathbf{u}_h, p_h)) - (\boldsymbol{\sigma}(\mathbf{u}_h, p_h) \mathbf{n}, (\mathbf{u}_h - \dot{\mathbf{d}}_h))_\Sigma \\ - (\boldsymbol{\sigma}(\mathbf{u}_h, -p_h) \mathbf{n}, \mathbf{u}_h - \dot{\mathbf{d}}_h)_\Sigma + \frac{\gamma \mu}{h} (\mathbf{u}_h - \dot{\mathbf{d}}_h, \mathbf{u}_h - \dot{\mathbf{d}}_h)_\Sigma + |(\mathbf{u}_h, p_h)|_S^2 \end{aligned}$$

for all  $\dot{\mathbf{d}}_h \in \mathbf{W}_h$  and  $(\mathbf{u}_h, p_h) \in \mathbf{V}_h \times Q_h$ .

**Proof.** Note that

$$\begin{aligned} A((\mathbf{u}_h, p_h), (\mathbf{u}_h, p_h)) - (\boldsymbol{\sigma}(\mathbf{u}_h, p_h) \mathbf{n}, (\mathbf{u}_h - \dot{\mathbf{d}}_h))_\Sigma - (\boldsymbol{\sigma}(\mathbf{u}_h, -p_h) \mathbf{n}, \mathbf{u}_h - \dot{\mathbf{d}}_h)_\Sigma \\ + \frac{\gamma \mu}{h} (\mathbf{u}_h - \dot{\mathbf{d}}_h, \mathbf{u}_h - \dot{\mathbf{d}}_h)_\Sigma + |(\mathbf{u}_h, p_h)|_S^2 \\ = \mu \|\boldsymbol{\epsilon}(\mathbf{u}_h)\|_{0, \Omega}^2 - 2(\boldsymbol{\sigma}(\mathbf{u}_h, 0) \mathbf{n}, (\mathbf{u}_h - \dot{\mathbf{d}}_h))_\Sigma + \gamma \mu \|\mathbf{u}_h - \dot{\mathbf{d}}_h\|_{\frac{1}{2}, h, \Sigma}^2 \\ + |(\mathbf{u}_h, p_h)|_S^2. \end{aligned}$$

We now observe that

$$(\boldsymbol{\sigma}(\mathbf{u}_h, 0) \mathbf{n}, \mathbf{u}_h - \dot{\mathbf{d}}_h)_\Sigma \leq \frac{C_T}{\gamma^{\frac{1}{2}}} \mu^{\frac{1}{2}} \|\boldsymbol{\epsilon}(\mathbf{u}_h)\|_{0, \Omega_T^f} \gamma^{\frac{1}{2}} \mu^{\frac{1}{2}} \|\mathbf{u}_h - \dot{\mathbf{d}}_h\|_{\frac{1}{2}, h, \Sigma}$$

and conclude using an arithmetic-geometric inequality with suitable weights, Lemma 1 and Korn's inequality.  $\square$  If we take  $\mathbf{v}_h = \mathbf{u}_h$ ,  $q_h = p_h$  and  $\mathbf{w}_h = \dot{\mathbf{d}}_h$  we then get the following energy inequality.

$$\begin{aligned} \frac{d}{dt} \left( \frac{\rho^f}{2} \|\mathbf{u}_h\|_{0, \Omega^f}^2 + \frac{\rho^s}{2} \|\dot{\mathbf{d}}_h\|_{0, \Omega^s}^2 + a^e(\mathbf{d}_h, \mathbf{d}_h) \right) \\ + c_s (\mu_S \|\boldsymbol{\epsilon}(\mathbf{u}_h)\|_{0, \Omega_T^h}^2 + \gamma \mu \|\mathbf{u}_h - \dot{\mathbf{d}}_h\|_{\frac{1}{2}, h, \Sigma}^2 + |(\mathbf{u}_h, p_h)|_S^2) \leq 0. \quad (11) \end{aligned}$$

### 3.2 Consistency of the formulation

If we multiply (1) by  $\mathbf{v}_h, q_h \in \mathbf{V} \times Q_h$  and (2) by  $\mathbf{w}_h$  and integrate by parts in both systems we obtain the equality

$$\begin{aligned} \rho^f (\partial_t \mathbf{u}, \mathbf{v}_h) + A((\mathbf{u}, p), (\mathbf{v}_h, q_h)) + \rho^s (\partial_t \dot{\mathbf{d}}, \mathbf{w}_h)_{\Omega^s} + a^e(\mathbf{d}, \mathbf{w}_h) \\ - (\boldsymbol{\sigma}(\mathbf{u}, p) \mathbf{n}, (\mathbf{v}_h - \mathbf{w}_h))_\Sigma = 0. \end{aligned}$$

In the integral on the interface we have used that

$$-(\boldsymbol{\sigma}^s(\mathbf{d}) \mathbf{n}, \mathbf{w}_h)_\Sigma = (\boldsymbol{\sigma}(\mathbf{u}, p) \mathbf{n}, \mathbf{w}_h)_\Sigma. \quad (12)$$

Recalling that  $\mathbf{u}|_\Sigma = \dot{\mathbf{d}}|_\Sigma$  we observe that we may write

$$\begin{aligned} & \rho^f(\partial_t \mathbf{u}, \mathbf{v}_h) + A((\mathbf{u}, p), (\mathbf{v}_h, q_h)) + \rho^s(\partial_t \dot{\mathbf{d}}, \mathbf{w}_h)_{\Omega^s} + a^e(\mathbf{d}, \mathbf{w}_h) \\ & - (\boldsymbol{\sigma}(\mathbf{u}, p)\mathbf{n}, (\mathbf{v}_h - \mathbf{w}_h))_\Sigma - ((\mathbf{u} - \dot{\mathbf{d}}), \boldsymbol{\sigma}(\mathbf{v}_h, -q_h)\mathbf{n})_\Sigma \\ & + \frac{\gamma\mu}{h}((\mathbf{u} - \dot{\mathbf{d}}), (\mathbf{v}_h - \mathbf{w}_h))_\Sigma = 0 \end{aligned} \quad (13)$$

for all  $\mathbf{v}_h, q_h, \mathbf{w}_h \in \mathbf{V}_h \times Q_h \times \mathbf{W}_h$ . Taking the difference between (13) and (10) we obtain the following result

**Lemma 3** (*Galerkin orthogonality*) *The formulation (10) satisfies the following approximate Galerkin orthogonality*

$$\begin{aligned} & \rho^f(\partial_t(\mathbf{u} - \mathbf{u}_h), \mathbf{v}_h) + A((\mathbf{u} - \mathbf{u}_h, p - p_h), (\mathbf{v}_h, q_h)) + \rho^s(\partial_t(\dot{\mathbf{d}} - \dot{\mathbf{d}}_h), \mathbf{w}_h)_{\Omega^s} \\ & + a^e(\mathbf{d} - \mathbf{d}_h, \mathbf{w}_h) - (\boldsymbol{\sigma}(\mathbf{u} - \mathbf{u}_h, p - p_h)\mathbf{n}, (\mathbf{v}_h - \mathbf{w}_h))_\Sigma \\ & - (((\mathbf{u} - \mathbf{u}_h) - (\dot{\mathbf{d}} - \dot{\mathbf{d}}_h)), \boldsymbol{\sigma}(\mathbf{v}_h, -q_h)\mathbf{n})_\Sigma \\ & + \frac{\gamma\mu}{h}(((\mathbf{u} - \mathbf{u}_h) - (\dot{\mathbf{d}} - \dot{\mathbf{d}}_h)), (\mathbf{v}_h - \mathbf{w}_h))_\Sigma = S_h((\mathbf{u}_h, p_h), (\mathbf{v}_h, q_h)) \end{aligned} \quad (14)$$

for all  $\mathbf{v}_h, q_h, \mathbf{w}_h \in \mathbf{V}_h \times Q_h \times \mathbf{W}_h$ .

### 3.3 Error analysis

We introduce the discrete solid errors  $\boldsymbol{\xi}_h \stackrel{\text{def}}{=} \mathbf{d}_h - \pi_h^e \mathbf{d}$ ,  $\dot{\boldsymbol{\xi}}_h \stackrel{\text{def}}{=} \dot{\mathbf{d}}_h - \mathcal{I}_h \dot{\mathbf{d}}$ , where  $\pi_h^e$  stands for the elastic Ritz-projection of the solid  $a_e(\mathbf{d} - \pi_h^e \mathbf{d}, \mathbf{v}_h) = 0$  for all  $\mathbf{v}_h \in \mathbf{W}_h$ . The interpolation operator  $\mathcal{I}_h$  is defined by

$$\mathcal{I}_h \dot{\mathbf{d}} \stackrel{\text{def}}{=} \pi_h^e \dot{\mathbf{d}} + \sum \alpha_i \boldsymbol{\varphi}_i.$$

The  $\boldsymbol{\varphi}_i$  are basis functions with support in the elements with faces intersecting the interface in the patches  $F_i$  and the  $\alpha_i \in \mathbb{R}$  are chosen so that

$$\int_{F_i} (\dot{\mathbf{d}} - \mathcal{I}_h \dot{\mathbf{d}}) \cdot \mathbf{n} = 0. \quad (15)$$

For details on the construction of  $\boldsymbol{\varphi}_i$  we refer to [2]. We now assume that there exist two linear continuous lifting operators  $E_2 : H^2(\Omega^f) \rightarrow H^2(\mathbb{R}^2)$  and  $E_1 : H^1(\Omega^f) \rightarrow H^1(\mathbb{R}^2)$ . Using these lifting operators we introduce the discrete errors for the fluid  $\boldsymbol{\theta}_h \stackrel{\text{def}}{=} \mathbf{u}_h - i_{sz} E_2 \mathbf{u}$ ,  $y_h \stackrel{\text{def}}{=} p_h - i_{sz} E_1 p$ , where  $i_{sz}$  is defined by the Scott-Zhang interpolant. We assume that the stabilization operator defined in (9) satisfies the following weak consistency property

$$|(i_{sz} E_2 \mathbf{u}(t), i_{sz} E_1 p(t))|_S \leq Ch(\mu^{\frac{1}{2}} |\mathbf{u}|_{2, \Omega^f} + \mu^{-\frac{1}{2}} |p|_{1, \Omega^f}). \quad (16)$$

For a proof of this property for the velocity part we refer to [9]. The pressure part is an immediate consequence of the  $H^1$ -stability of the Scott-Zhang interpolant and the stability of the extension operator  $E_1$ ,

$$s_p(i_{sz} E_1 p(t), i_{sz} E_1 p(t))^{\frac{1}{2}} \lesssim \mu^{-\frac{1}{2}} h |i_{sz} E_1 p|_{1, \Omega^f} \lesssim \mu^{-\frac{1}{2}} h |E_1 p|_{1, \Omega^f} \lesssim \mu^{-\frac{1}{2}} h |p|_{1, \Omega^f}.$$

The remaining necessary approximation estimates for these interpolants are collected in the following Lemma.

**Lemma 4** Assume that  $\mathbf{d}, \dot{\mathbf{d}} \in H^2(\Omega^s)$ ,  $\mathbf{u} \in H^2(\Omega^f)$  and  $p \in H^1(\Omega^f)$  then the following error estimate holds

$$\begin{aligned} & \|\mathbf{u} - i_{sz}E_2\mathbf{u}\|_{0,\Omega^f} + h\|\nabla(\mathbf{u} - i_{sz}E_2\mathbf{u})\|_{0,\Omega^f} \lesssim h^2|\mathbf{u}|_{2,\Omega^f} \\ & \|p - i_{sz}E_1p\|_{0,\Omega^f} + h\|\nabla(p - i_{sz}E_1p)\|_{0,\Omega^f} \lesssim h|p|_{1,\Omega^f}, \\ & \|\mathbf{d} - \pi_h^e\mathbf{d}\|_{0,\Omega^s} + h\|\nabla(\mathbf{d} - \pi_h^e\mathbf{d})\|_{0,\Omega^s} \lesssim h^2|\mathbf{d}|_{2,\Omega^s}, \\ & \|\dot{\mathbf{d}} - \mathcal{I}_h\dot{\mathbf{d}}\|_{0,\Omega^s} + h\|\nabla(\dot{\mathbf{d}} - \mathcal{I}_h\dot{\mathbf{d}})\|_{0,\Omega^s} \lesssim h^2|\dot{\mathbf{d}}|_{2,\Omega^s}, \\ & \|\boldsymbol{\sigma}(\mathbf{u} - i_{sz}E_2\mathbf{u}, p - i_{sz}E_1p)\mathbf{n}\|_{-\frac{1}{2},h,\Sigma} \lesssim h(\|\mathbf{u}\|_{2,\Omega^f} + \|p\|_{1,\Omega^f}) \\ & \|(\mathbf{u} - i_{sz}E_2\mathbf{u}) - (\dot{\mathbf{d}} - \mathcal{I}_h\dot{\mathbf{d}})\|_{\frac{1}{2},h,\Sigma} \lesssim h(\|\mathbf{u}\|_{2,\Omega^f} + \|\dot{\mathbf{d}}\|_{2,\Omega^s}) \end{aligned}$$

**Proof.** We only discuss the proof of the three last estimates, since the other estimates follow using standard approximation theory and the stability of the extension operator. By the construction of  $\mathcal{I}_h$  we have,

$$\alpha_i = \frac{\int_{F_i} (\dot{\mathbf{d}} - \pi_h^e\dot{\mathbf{d}}) \cdot \mathbf{n}}{\int_{F_i} \boldsymbol{\varphi}_i \cdot \mathbf{n}}.$$

Since  $|\int_{F_i} \boldsymbol{\varphi}_i \cdot \mathbf{n}| \geq Ch$ , we have

$$|\alpha_i| \lesssim \frac{|\int_{F_i} (\dot{\mathbf{d}} - \pi_h^e\dot{\mathbf{d}}) \cdot \mathbf{n}|}{h} \leq h^{-\frac{1}{2}}\|\dot{\mathbf{d}} - \pi_h^e\dot{\mathbf{d}}\|_{0,F_i} \lesssim h^2|\dot{\mathbf{d}}|_{2,\Omega^s}. \quad (17)$$

Hence,

$$\|\dot{\mathbf{d}} - \mathcal{I}_h\dot{\mathbf{d}}\|_{0,\Omega^s} \leq \|\dot{\mathbf{d}} - \pi_h^e\dot{\mathbf{d}}\| + \sum \|\alpha_i\boldsymbol{\varphi}_i\|_{0,P_i} \lesssim h^2,$$

which ensures optimal approximability. For the error estimates on the trace  $\Sigma$ , note that we have

$$\|\boldsymbol{\sigma}(\mathbf{u} - i_{sz}E_2\mathbf{u}, p - i_{sz}E_1p)\mathbf{n}\|_{-\frac{1}{2},h,\Sigma} \lesssim h^{\frac{1}{2}}\|\nabla(\mathbf{u} - i_{sz}E_2\mathbf{u})\|_{0,\Sigma} + h^{\frac{1}{2}}\|p - i_{sz}E_1p\|_{0,\Sigma}$$

and

$$\|(\mathbf{u} - i_{sz}E_2\mathbf{u}) - (\dot{\mathbf{d}} - \mathcal{I}_h\dot{\mathbf{d}})\|_{\frac{1}{2},h,\Sigma} \lesssim h^{-\frac{1}{2}}(\|\mathbf{u} - i_{sz}E_2\mathbf{u}\|_{0,\Sigma} + \|\dot{\mathbf{d}} - \mathcal{I}_h\dot{\mathbf{d}}\|_{0,\Sigma}).$$

The quantities on the solid side where the mesh is fitted to interface are treated in a standard fashion using element-wise trace inequalities. We will detail the estimates for quantities on the unfitted mesh. Using the trace inequality (5) element wise for all elements intersected by the interface we have

$$\begin{aligned} & h^{\frac{1}{2}}\|\nabla(\mathbf{u} - i_{sz}E_2\mathbf{u})\|_{0,\Sigma} + h^{-\frac{1}{2}}\|\mathbf{u} - i_{sz}E_2\mathbf{u}\|_{0,\Sigma} \\ & \lesssim h|E_2\mathbf{u}|_{2,\Sigma} + \|\nabla(\mathbf{u} - i_{sz}E_2\mathbf{u})\|_{0,\Omega_\tau^f} + h^{-1}\|\mathbf{u} - i_{sz}E_2\mathbf{u}\|_{0,\Omega_\tau^f} \lesssim h|E_2\mathbf{u}|_{2,\Omega_\tau^f} \\ & \lesssim h|\mathbf{u}|_{2,\Omega^f} \end{aligned}$$

where the last inequality is a consequence of the stability of the extension operator. Similarly we may estimate the trace error of the pressure in the following fashion

$$\begin{aligned} & h^{\frac{1}{2}}\|p - i_{sz}E_1p\|_{0,\Sigma} \lesssim \|\nabla(p - i_{sz}E_1p)\|_{0,\Omega_\tau^f} + h^{-1}\|p - i_{sz}E_1p\|_{0,\Omega_\tau^f} \lesssim h|E_1p|_{1,\Omega_\tau^f} \\ & \lesssim h|p|_{1,\Omega^f}. \end{aligned}$$

□ From (10) and (1)-(2) and by using Lemma 2, get the following perturbation equation for  $\boldsymbol{\theta}_h, \dot{\boldsymbol{\xi}}_h, \boldsymbol{\xi}_h$ ,

$$\begin{aligned}
& \frac{\rho^f}{2} \|\boldsymbol{\theta}_h\|_{0,\Omega^f}^2 + \frac{\rho^s}{2} \|\dot{\boldsymbol{\xi}}_h\|_{0,\Omega^s}^2 + \frac{1}{2} \|\boldsymbol{\xi}_h\|_e^2 \\
& + c_s \int_0^t \left[ \mu_f \|\nabla \boldsymbol{\theta}_h\|_{0,\Omega^f}^2 + \gamma \mu \|\boldsymbol{\theta}_h - \dot{\boldsymbol{\xi}}_h\|_{\frac{1}{2},h,\Sigma}^2 + |(\boldsymbol{\theta}_h, y_h)|_S^2 + a^e(\boldsymbol{\xi}_h, \dot{\boldsymbol{\xi}}_h - \partial_t \boldsymbol{\xi}_h) \right] \\
& \leq \frac{\rho^f}{2} \|\boldsymbol{\theta}_h(0)\|_{0,\Omega^f}^2 + \frac{\rho^s}{2} \|\dot{\boldsymbol{\xi}}_h(0)\|_{0,\Omega^s}^2 + \frac{1}{2} \|\boldsymbol{\xi}_h(0)\|_e^2 \\
& + \int_0^t \left[ \rho^f (\partial_t \boldsymbol{\theta}_h, \boldsymbol{\theta}_h)_{\Omega^f} + \rho^s (\partial_t \dot{\boldsymbol{\xi}}_h, \dot{\boldsymbol{\xi}}_h) + |(\boldsymbol{\theta}_h, y_h)|_S^2 \right. \\
& + A\left((\boldsymbol{\theta}_h, y_h), (\boldsymbol{\theta}_h, y_h)\right) - (\boldsymbol{\sigma}(\boldsymbol{\theta}_h, y_h) \mathbf{n}, (\boldsymbol{\theta}_h - \dot{\boldsymbol{\xi}}_h))_{\Sigma} - (\boldsymbol{\sigma}(\boldsymbol{\theta}_h, -y_h) \mathbf{n}, \boldsymbol{\theta}_h - \dot{\boldsymbol{\xi}}_h)_{\Sigma} \\
& \left. + \frac{\gamma \mu}{h} (\boldsymbol{\theta}_h - \dot{\boldsymbol{\xi}}_h, \boldsymbol{\theta}_h - \dot{\boldsymbol{\xi}}_h)_{\Sigma} + a^e(\boldsymbol{\xi}_h, \dot{\boldsymbol{\xi}}_h) \right]. \quad (18)
\end{aligned}$$

Observe that due to the different definition of the interpolation operators in  $\boldsymbol{\xi}_h$  and  $\dot{\boldsymbol{\xi}}_h$ , it does not hold that  $\dot{\boldsymbol{\xi}}_h = \partial_t \boldsymbol{\xi}_h$ . Therefore to obtain the above inequality we used the fact that

$$\frac{1}{2} \|\boldsymbol{\xi}_h\|_e^2 - \frac{1}{2} \|\boldsymbol{\xi}_h(0)\|_e^2 + \int_0^t a^e(\boldsymbol{\xi}_h, \dot{\boldsymbol{\xi}}_h - \partial_t \boldsymbol{\xi}_h) dt = \int_0^t a^e(\boldsymbol{\xi}_h, \dot{\boldsymbol{\xi}}_h) dt.$$

This results in a non-positive contribution  $a^e(\boldsymbol{\xi}_h, \dot{\boldsymbol{\xi}}_h - \partial_t \boldsymbol{\xi}_h)$  in the left hand side of (18) which will be treated as an approximation error in the error analysis below. Note that the pressure is only controlled in the weak norm given by the stabilization operator. In the analysis below it is convenient to denote the approximation errors by

$$\boldsymbol{\theta}_\pi \stackrel{\text{def}}{=} E_2 \mathbf{u} - i_{sz} E_2 \mathbf{u}, \quad y_\pi \stackrel{\text{def}}{=} E_1 y - i_{sz} E_1 p \quad \text{in } \Omega_{\mathcal{T}}^f$$

and

$$\boldsymbol{\xi}_\pi \stackrel{\text{def}}{=} \mathbf{d} - \pi_e \mathbf{d}, \quad \dot{\boldsymbol{\xi}}_\pi \stackrel{\text{def}}{=} \dot{\mathbf{d}} - \pi_e \dot{\mathbf{d}} \quad \text{in } \Omega^s.$$

We are now ready to state and prove the main result of this note.

**Theorem 5** *Let  $\mathbf{u}, p$  be the solution of (1) and  $\mathbf{d}, \dot{\mathbf{d}}$  be the solution of (2). Assume that the exact solution has the regularity required by the approximation results of Lemma 4. Then there holds*

$$\begin{aligned}
& \frac{\rho^f}{2} \|\mathbf{u}_h - \mathbf{u}\|_{0,\Omega^f}^2 + \frac{\rho^s}{2} \|\dot{\mathbf{d}}_h - \dot{\mathbf{d}}\|_{0,\Omega^s}^2 + \frac{1}{2} \|\mathbf{d}_h - \mathbf{d}\|_e^2 \\
& + c_s \int_0^t \left[ \mu_f \|\nabla(\mathbf{u}_h - \mathbf{u})\|_{0,\Omega^f}^2 + \gamma \mu \|\mathbf{u}_h - \dot{\mathbf{d}}_h\|_{\frac{1}{2},h,\Sigma}^2 \right] dt \lesssim h^2.
\end{aligned}$$

**Proof.** By a triangle inequality and the optimal approximability of the proposed interpolants it is sufficient to prove the convergence of the discrete error. Consider first the inequality (18). After applying the Galerkin orthogonality (14) in the right hand side and noting that  $a^e(\boldsymbol{\xi}_\pi, \dot{\boldsymbol{\xi}}_h) = 0$ ,

we have

$$\begin{aligned}
& \frac{\rho^f}{2} \|\boldsymbol{\theta}_h\|_{0,\Omega^f}^2 + \frac{\rho^s}{2} \|\dot{\boldsymbol{\xi}}_h\|_{0,\Omega^s}^2 + \frac{1}{2} \|\boldsymbol{\xi}_h\|_e^2 \\
& \quad + c_s \int_0^t \left[ \mu_f \|\nabla \boldsymbol{\theta}_h\|_{0,\Omega_T^f}^2 + \gamma \mu \|\boldsymbol{\theta}_h - \dot{\boldsymbol{\xi}}_h\|_{\frac{1}{2},h,\Sigma}^2 + |(\boldsymbol{\theta}_h, \mathbf{y}_h)|_S^2 \right] \\
& \quad \leq \frac{\rho^f}{2} \|\boldsymbol{\theta}_h(0)\|_{0,\Omega^f}^2 + \frac{\rho^s}{2} \|\dot{\boldsymbol{\xi}}_h(0)\|_{0,\Omega^s}^2 + \frac{1}{2} \|\boldsymbol{\xi}_h(0)\|_e^2 \\
& \quad + \int_0^t \left[ \underbrace{(\partial_t \boldsymbol{\theta}_\pi, \boldsymbol{\theta}_h)_{\Omega^f}}_{T_1} + (\partial_t \dot{\boldsymbol{\xi}}_\pi, \dot{\boldsymbol{\xi}}_h) + \underbrace{S_h((i_{sz} E_2 \mathbf{u}(t), i_{sz} E_1 p(t)), (\boldsymbol{\theta}_h, \mathbf{y}_h))}_{T_2} \right. \\
& \quad \left. \underbrace{A((\boldsymbol{\theta}_\pi, \mathbf{y}_\pi), (\boldsymbol{\theta}_h, \mathbf{y}_h)) - (\boldsymbol{\sigma}(\boldsymbol{\theta}_\pi, \mathbf{y}_\pi) \mathbf{n}, (\boldsymbol{\theta}_h - \dot{\boldsymbol{\xi}}_h))_\Sigma - (\boldsymbol{\sigma}(\boldsymbol{\theta}_h, \mathbf{y}_h) \mathbf{n}, \boldsymbol{\theta}_\pi - \dot{\boldsymbol{\xi}}_\pi)_\Sigma}_{T_3} \right. \\
& \quad \left. + \underbrace{\frac{\gamma \mu}{h} (\boldsymbol{\theta}_\pi - \dot{\boldsymbol{\xi}}_\pi, \boldsymbol{\theta}_h - \dot{\boldsymbol{\xi}}_h)_\Sigma}_{T_4} - \underbrace{a^e(\boldsymbol{\xi}_h, \dot{\boldsymbol{\xi}}_h - \partial_t \boldsymbol{\xi}_h)}_{T_5} \right]. \quad (19)
\end{aligned}$$

We may know bound the terms  $T_1, \dots, T_5$  term by term. Mainly by applying Cauchy-Schwarz inequality followed by trace inequalities and approximation.

$$\begin{aligned}
\int_0^t T_1 & \leq \rho^f \|\partial_t \boldsymbol{\theta}_\pi\|_{L^2(0,t;\Omega^f)} \|\boldsymbol{\theta}_h\|_{L^2(0,t;\Omega^f)} + \|\partial_t \dot{\boldsymbol{\xi}}_\pi\|_{L^2(0,t;\Omega^f)} \|\dot{\boldsymbol{\xi}}_h\|_{L^2(0,t;\Omega^s)} \\
& \leq Ch^4 (\rho^f \|\partial_t \mathbf{u}\|_{L^2(0,t;H^2(\Omega^f))}^2 + \rho^s \|\partial_t \mathbf{d}\|_{L^2(0,t;H^2(\Omega^s))}^2) + \rho^f \|\boldsymbol{\theta}_h\|_{L^2(0,t;\Omega^f)}^2 \\
& \quad + \rho^s \|\dot{\boldsymbol{\xi}}_h\|_{L^2(0,t;\Omega^s)}^2.
\end{aligned}$$

The two first terms in the right hand side have optimal convergence order and the last two may be controlled using Gronwall's lemma. For  $T_2$  we observe that

$$\int_0^t T_2 \leq \frac{1}{2c_s} \int_0^t |i_{sz} E_2 \mathbf{u}(t), i_{sz} E_1 p(t)|_S^2 + \frac{c_s}{2} \int_0^t |(\boldsymbol{\theta}_h, \mathbf{y}_h)|_S^2$$

where the second term in the right hand side is absorbed in the left hand side of (25) and the first term is bounded using the approximation (16). To bound  $T_3$  first note that the second term in the expression is bounded in by the Cauchy-Schwarz inequality followed by approximation

$$\begin{aligned}
\int_0^t |(\boldsymbol{\sigma}(\boldsymbol{\theta}_\pi, \mathbf{y}_\pi) \mathbf{n}, (\boldsymbol{\theta}_h - \dot{\boldsymbol{\xi}}_h))_\Sigma| & \leq Ch^2 (|\mathbf{u}|_{L^2(0,t;H^2(\Omega^f))}^2 + |p|_{L^2(0,t;H^1(\Omega^f))}^2) \\
& \quad + \frac{c_s}{4} \gamma \mu \int_0^t \|\boldsymbol{\theta}_h - \dot{\boldsymbol{\xi}}_h\|_{\frac{1}{2},h,\Sigma}^2. \quad (20)
\end{aligned}$$

We then consider the velocity part and observe that

$$\begin{aligned}
& \int_0^t (a(\boldsymbol{\theta}_\pi, \boldsymbol{\theta}_h) - (\boldsymbol{\sigma}(\boldsymbol{\theta}_h, 0) \mathbf{n}, \boldsymbol{\theta}_\pi - \dot{\boldsymbol{\xi}}_\pi)_\Sigma) \\
& \quad \leq Ch^2 (\|\mathbf{u}\|_{L^2(0,t;H^2(\Omega^f))}^2 + \|\mathbf{d}\|_{L^2(0,t;H^2(\Omega^s))}^2) + \frac{c_s}{2} \mu \int_0^t \|\nabla \boldsymbol{\theta}_h\|_{0,\Omega_T^f}^2. \quad (21)
\end{aligned}$$

The pressure velocity coupling is the most interesting part of the continuity. For the remaining terms of  $T_3$  we write, using an integration by parts in the mass conservation equation,

$$\begin{aligned} & b(y_\pi, \boldsymbol{\theta}_h) - b(y_h, \boldsymbol{\theta}_\pi) - (\boldsymbol{\sigma}(0, -y_h)\mathbf{n}, \boldsymbol{\theta}_\pi - \dot{\boldsymbol{\xi}}_\pi)_\Sigma \\ &= (y_\pi, \nabla \cdot \boldsymbol{\theta}_h)_{\Omega^f} - (y_h, \nabla \cdot \boldsymbol{\theta}_\pi)_{\Omega^f} - (\boldsymbol{\sigma}(0, -y_h)\mathbf{n}, \boldsymbol{\theta}_\pi - \dot{\boldsymbol{\xi}}_\pi)_\Sigma \\ &= \underbrace{(y_\pi, \nabla \cdot \boldsymbol{\theta}_h)_{\Omega^f}}_{T_{31}} - \underbrace{(\nabla y_h, \boldsymbol{\theta}_\pi)_{\Omega^f}}_{T_{32}} - \underbrace{(\boldsymbol{\sigma}(0, y_h)\mathbf{n}, \dot{\boldsymbol{\xi}}_\pi)_\Sigma}_{T_{33}}. \end{aligned} \quad (22)$$

Estimating the terms  $T_{31} - T_{33}$  we get

$$\begin{aligned} \int_0^t T_{31} &\leq Ch^2 |p|_{L^2(0,t;H^1(\Omega^f))}^2 + \frac{c_s}{4} \int_0^t \|\nabla \boldsymbol{\theta}_h\|_{0,\Omega^f}^2, \\ \int_0^t T_{32} &\leq Ch^2 \|\mathbf{u}\|_{L^2(0,t;H^2(\Omega^f))}^2 + \frac{c_s}{8} \int_0^t |(0, y_h)|_S^2. \end{aligned}$$

Denoting by  $y_i$  the average of  $y_h$  over the interface patch  $F_i$  we obtain using the property (15) of the interpolant  $\mathcal{I}_h$ ,

$$\begin{aligned} T_{33} &= \sum_i (y_h - y_i, \dot{\boldsymbol{\xi}}_\pi \cdot \mathbf{n})_{F_i} \leq C \|h \nabla y_h\|_{0,\Omega^f} h \|\dot{\mathbf{d}}\|_{H^2(\Omega^s)} \\ &\leq \frac{c_s}{8} |(0, y_h)|_S^2 + Ch^2 \|\dot{\mathbf{d}}\|_{H^2(\Omega^s)}^2. \end{aligned} \quad (23)$$

The boundary penalty term  $T_4$  is handled using Cauchy-Schwarz inequality followed by approximation,

$$\begin{aligned} \int_0^t T_4 &\leq \frac{1}{c_s} \gamma \mu \int_0^t \|\boldsymbol{\theta}_\pi - \dot{\boldsymbol{\xi}}_\pi\|_{\frac{1}{2},h,\Sigma}^2 + \frac{c_s}{4} \gamma \mu \int_0^t \|\boldsymbol{\theta}_h - \dot{\boldsymbol{\xi}}_h\|_{\frac{1}{2},h,\Sigma}^2 \\ &\leq \frac{1}{c_s} \gamma \mu h^2 (\|\mathbf{u}\|_{L^2(0,t;H^2(\Omega^f))}^2 + \|\dot{\mathbf{d}}\|_{L^2(0,t;H^2(\Omega^s))}^2) + \frac{c_s}{4} \gamma \mu \int_0^t \|\boldsymbol{\theta}_h - \dot{\boldsymbol{\xi}}_h\|_{\frac{1}{2},h,\Sigma}^2 \end{aligned} \quad (24)$$

we see that the first term has the right convergence order and the second term can be absorbed in the left hand side of (25). The last term  $T_5$  finally is bounded using the fact that  $\dot{\boldsymbol{\xi}}_h - \partial_t \boldsymbol{\xi}_h = \sum_i \alpha_i \boldsymbol{\varphi}_i$  and the convergence order of the perturbation is known (c.f. equation (17)),

$$\begin{aligned} \int_0^t T_5 &= \int_0^t a^e(\boldsymbol{\xi}_h, \dot{\boldsymbol{\xi}}_h - \partial_t \boldsymbol{\xi}_h) = \sum_i \int_0^t a^e(\boldsymbol{\xi}_h, \alpha_i \boldsymbol{\varphi}_i) \leq \sum_i \int_0^t \|\boldsymbol{\xi}_h\|_e \|\alpha_i \boldsymbol{\varphi}_i\|_{1,\Omega^s} \\ &\lesssim \int_0^t \|\boldsymbol{\xi}_h\|_e^2 + h^2 \|\dot{\mathbf{d}}\|_{L^2(0,t;H^2(\Omega^s))}^2. \end{aligned}$$

We may now collect the above bounds and conclude by applying Gronwall's lemma on the following system

$$\begin{aligned}
& \frac{\rho^f}{2} \|\boldsymbol{\theta}_h\|_{0,\Omega^f}^2 + \frac{\rho^s}{2} \|\dot{\boldsymbol{\xi}}_h\|_{0,\Omega^s}^2 + \frac{1}{2} \|\boldsymbol{\xi}_h\|_e^2 \\
& \quad + \frac{c_s}{4} \int_0^t \left[ \mu_f \|\nabla \boldsymbol{\theta}_h\|_{0,\Omega^f_\tau}^2 + \gamma \mu \|\boldsymbol{\theta}_h - \dot{\boldsymbol{\xi}}_h\|_{\frac{1}{2},h,\Sigma}^2 + |(\boldsymbol{\theta}_h, \mathbf{y}_h)|_S^2 \right] \\
& \quad \leq \frac{\rho^f}{2} \|\boldsymbol{\theta}_h(0)\|_{0,\Omega^f}^2 + \frac{\rho^s}{2} \|\dot{\boldsymbol{\xi}}_h(0)\|_{0,\Omega^s}^2 + \frac{1}{2} \|\boldsymbol{\xi}_h(0)\|_e^2 \\
& \quad + Cth^4 (\rho^f \|\partial_t \mathbf{u}\|_{L^2(0,t;H^2(\Omega^f))}^2 + \rho^s \|\partial_t \dot{\mathbf{d}}\|_{L^2(0,t;H^2(\Omega^s))}^2) \\
& \quad + Cth^2 (\|\mathbf{u}\|_{L^2(0,t;H^2(\Omega^f))}^2 + \|p\|_{L^2(0,t;H^1(\Omega^f))}^2 + \|\dot{\mathbf{d}}\|_{L^2(0,t;H^2(\Omega^s))}^2) \\
& \quad + t^{-1} (\rho^f \|\boldsymbol{\theta}_h\|_{L^2(0,t;\Omega^f)}^2 + \rho^s \|\dot{\boldsymbol{\xi}}_h\|_{L^2(0,t;\Omega^s)}^2 + \int_0^t \|\boldsymbol{\xi}_h\|_e^2). \quad (25)
\end{aligned}$$

□

## 4 Time discretization: coupling schemes

This section is devoted to the time discretization of the space semi-discrete formulation (10). Both implicit and explicit coupling strategies are discussed. In the subsequent text, the parameter  $\tau > 0$  stands for the time-step length,  $t_n \stackrel{\text{def}}{=} n\tau$ , for  $n \in \mathbb{N}$  and  $\partial_\tau x^n \stackrel{\text{def}}{=} (x^n - x^{n-1})/\tau$  for the first-order backward difference. We also introduce the fluid discrete bi-linear form

$$a_h^f((\mathbf{u}_h, p_h), (\mathbf{v}_h, q_h)) \stackrel{\text{def}}{=} A((\mathbf{u}_h, p_h), (\mathbf{v}_h, q_h)) + S_h((\mathbf{u}_h, p_h), (\mathbf{v}_h, q_h)).$$

### 4.1 Implicit coupling

An overall implicit first-order scheme is considered for the time-discretization of (10). This yields the following time-advancing procedure reported in Algorithm 1.

---

#### Algorithm 1 Implicit coupling scheme

---

For  $n \geq 1$ , find  $(\mathbf{u}_h^n, p_h^n, \dot{\mathbf{d}}_h^n, \mathbf{d}_h^n) \in \mathbf{V}_h \times Q_h \times \mathbf{W}_h \times \mathbf{W}_h$ , such that  $\dot{\mathbf{d}}_h^n = \partial_\tau \mathbf{d}_h^n$  and

$$\begin{cases} \rho^f (\partial_\tau \mathbf{u}_h^n, \mathbf{v}_h) + a_h^f((\mathbf{u}_h^n, p_h^n), (\mathbf{v}_h, q_h)) + \rho^s (\partial_\tau \dot{\mathbf{d}}_h^n, \mathbf{w}_h)_{\Omega^s} + a^e(\mathbf{d}_h^n, \mathbf{w}_h) \\ \quad - (\boldsymbol{\sigma}(\mathbf{u}_h^n, p_h^n) \mathbf{n}, (\mathbf{v}_h - \mathbf{w}_h))_\Sigma - ((\mathbf{u}_h^n - \dot{\mathbf{d}}_h^n), \boldsymbol{\sigma}(\mathbf{v}_h, -q_h) \mathbf{n})_\Sigma \\ \quad + \frac{\gamma \mu}{h} ((\mathbf{u}_h^n - \dot{\mathbf{d}}_h^n), (\mathbf{v}_h - \mathbf{w}_h))_\Sigma = 0 \end{cases} \quad (26)$$

for all  $(\mathbf{v}_h, q_h, \mathbf{w}_h) \in \mathbf{V}_h \times Q_h \times \mathbf{W}_h$ .

---

Note that at, at each time level  $n$ , the fluid  $(\mathbf{u}_h^n, p_h^n)$  and solid  $(\dot{\mathbf{d}}_h^n, \mathbf{d}_h^n)$  states are fully coupled. The next results states the unconditional stability of the implicit scheme given by (26), and where

$$E^n \stackrel{\text{def}}{=} \frac{\rho^f}{2} \|\mathbf{u}_h^n\|_{0,\Omega^f}^2 + \frac{\rho^s}{2} \|\dot{\mathbf{d}}_h^n\|_{0,\Omega^s}^2 + a^e(\mathbf{d}_h^n, \mathbf{d}_h^n),$$

denotes the total energy of the discrete system a time  $t_n$ .

**Lemma 6** Let  $\{(\mathbf{u}_h^n, p_h^n, \dot{\mathbf{d}}_h^n, \mathbf{d}_h^n)\}_{n \geq 1}$  be the sequence given by Algorithm 1. Then, under the condition  $\gamma > C_T^2$ , there holds  $E^n \leq E^0$  for all  $n \geq 1$ .

**Proof.** The result is a straightforward consequence of Lemma 2, after taking  $(\mathbf{v}_h, q_h, \mathbf{w}_h) = (\mathbf{u}_h^n, p_h^n, \dot{\mathbf{d}}_h^n)$  in (26).  $\square$

## 4.2 Explicit coupling

In this paragraph we introduce time-marching procedures that allow an uncoupled computation of the fluid  $(\mathbf{u}_h^n, p_h^n)$  and solid  $(\dot{\mathbf{d}}_h^n, \mathbf{d}_h^n)$  states (explicit coupling schemes). Basically, the proposed methods generalized the Nitsche based splitting schemes, introduced in [6, 7], to the unfitted framework provided by (10). To this purpose, we first note that the monolithic problem (10) can be equivalently formulated in terms of two coupled sub-problems: for  $t > 0$

- Solid sub-problem: find  $(\dot{\mathbf{d}}_h(t), \mathbf{d}_h(t)) \in \mathbf{W}_h \times \mathbf{W}_h$  with  $\dot{\mathbf{d}}_h(t) = \partial_t \mathbf{d}_h(t)$  and such that

$$\begin{aligned} \rho^s (\partial_t \dot{\mathbf{d}}_h, \mathbf{w}_h)_{\Omega^s} + a^e(\mathbf{d}_h, \mathbf{w}_h) + \frac{\gamma^\mu}{h} (\dot{\mathbf{d}}_h, \mathbf{w}_h)_\Sigma \\ = -\frac{\gamma^\mu}{h} (\mathbf{u}_h, \mathbf{w}_h)_\Sigma - (\boldsymbol{\sigma}(\mathbf{u}_h, p_h) \mathbf{n}, \mathbf{w}_h)_\Sigma \end{aligned} \quad (27)$$

for all  $\mathbf{w}_h \in \mathbf{W}_h$ .

- Fluid sub-problem: find  $(\mathbf{u}_h(t), p_h(t)) \in \mathbf{V}_h \times Q_h$  such that

$$\begin{aligned} \rho^f (\partial_t \mathbf{u}_h, \mathbf{v}_h)_{\Omega^f} + a_h^f((\mathbf{u}_h, p_h), (\mathbf{v}_h, q_h)) - ((\mathbf{u}_h - \dot{\mathbf{d}}_h), \boldsymbol{\sigma}(\mathbf{v}_h, -q_h) \mathbf{n})_\Sigma \\ + \frac{\gamma^\mu}{h} (\mathbf{u}_h, \mathbf{v}_h)_\Sigma = \frac{\gamma^\mu}{h} (\dot{\mathbf{d}}_h, \mathbf{v}_h)_\Sigma + (\boldsymbol{\sigma}(\mathbf{u}_h, p_h) \mathbf{n}, \mathbf{v}_h)_\Sigma \end{aligned} \quad (28)$$

for all  $(\mathbf{v}_h, q_h) \in \mathbf{V}_h \times Q_h$ .

---

### Algorithm 2 Stabilized explicit coupling scheme

---

For  $n \geq 1$ :

1. Solid sub-step: find  $(\dot{\mathbf{d}}_h^n, \mathbf{d}_h^n) \in \mathbf{W}_h \times \mathbf{W}_h$  with  $\dot{\mathbf{d}}_h^n = \partial_\tau \mathbf{d}_h^n$  and such that

$$\begin{aligned} \rho^s (\partial_\tau \dot{\mathbf{d}}_h^n, \mathbf{w}_h)_{\Omega^s} + a^e(\mathbf{d}_h^n, \mathbf{w}_h) + \frac{\gamma^\mu}{h} (\dot{\mathbf{d}}_h^n, \mathbf{w}_h)_\Sigma \\ = -\frac{\gamma^\mu}{h} (\mathbf{u}_h^{n-1}, \mathbf{w}_h)_\Sigma - (\boldsymbol{\sigma}(\mathbf{u}_h^{n-1}, p_h^{n-1}) \mathbf{n}, \mathbf{w}_h)_\Sigma \end{aligned} \quad (29)$$

for all  $\mathbf{w}_h \in \mathbf{W}_h$ .

2. Fluid sub-step: find  $(\mathbf{u}_h^n, p_h^n) \in \mathbf{V}_h \times Q_h$  such that

$$\begin{aligned} \rho^f (\partial_\tau \mathbf{u}_h^n, \mathbf{v}_h)_{\Omega^f} + a_h^f((\mathbf{u}_h^n, p_h^n), (\mathbf{v}_h, q_h)) - (\mathbf{u}_h^n - \dot{\mathbf{d}}_h^n, q_h \mathbf{n})_\Sigma + \frac{\gamma^\mu}{h} (\mathbf{u}_h^n, \mathbf{v}_h)_\Sigma \\ + \frac{\gamma_0 h}{\gamma^\mu} (p_h^n - p_h^{n-1}, q_h)_\Sigma = \frac{\gamma^\mu}{h} (\dot{\mathbf{d}}_h^n, \mathbf{v}_h)_\Sigma + (\boldsymbol{\sigma}(\mathbf{u}_h^{n-1}, p_h^{n-1}) \mathbf{n}, \mathbf{v}_h)_\Sigma \end{aligned} \quad (30)$$

for all  $(\mathbf{v}_h, q_h) \in \mathbf{V}_h \times Q_h$ .

---

Following [6, 7], we propose to uncoupled the time-marching of (27) and (28) through the explicit treatment of the interface fluid terms in (27), as detailed in Algorithm 2. Note that, in the fluid sub-step (30), the interface fluid stress is explicitly treated. This explains why the symmetrizing viscous term

$$((\mathbf{u}_h^n - \mathbf{d}_h^n), \boldsymbol{\sigma}(\mathbf{v}_h, 0)\mathbf{n})_\Sigma,$$

is missing in (30). The weakly consistent interface pressure stabilization,

$$\frac{\gamma_0 h}{\gamma \mu} (p_h^n - p_h^{n-1}, q_h)_\Sigma, \quad \gamma_0 > 0,$$

is introduced to control the artificial interface pressure fluctuations induced by the splitting of pressure stress in time.

---

**Algorithm 3** Stabilized explicit coupling scheme with  $K$ -correction steps
 

---

For  $n \geq 2$ :

1. Extrapolation:

$$\mathbf{u}_h^{n,0} = 2\mathbf{u}_h^{n-1} - \mathbf{u}_h^{n-2}, \quad \boldsymbol{\sigma}(\mathbf{u}_h^{n,0}, p_h^{n,0})\mathbf{n} = \boldsymbol{\sigma}(\mathbf{u}_h^{n-1}, p_h^{n-1})\mathbf{n}, \quad p_h^{n,0} = p_h^{n-1}. \quad (31)$$

2. For  $k = 1, \dots, K + 1$ :

- Solid sub-step: find  $(\mathbf{d}_h^{n,k}, \mathbf{d}_h^{n,k}) \in \mathbf{W}_h \times \mathbf{W}_h$ , with  $\mathbf{d}_h^{n,k} = (\mathbf{d}_h^{n,k} - \mathbf{d}_h^{n-1})/\tau$  and such that

$$\begin{aligned} \rho^s(\partial_\tau \mathbf{d}_h^{n,k}, \mathbf{w}_h)_{\Omega^s} + a^e(\mathbf{d}_h^{n,k}, \mathbf{w}_h) + \frac{\gamma \mu}{h} (\mathbf{d}_h^{n,k}, \mathbf{w}_h)_\Sigma \\ = -\frac{\gamma \mu}{h} (\mathbf{u}_h^{n,k-1}, \mathbf{w}_h)_\Sigma - (\boldsymbol{\sigma}^{n,k-1}\mathbf{n}, \mathbf{w}_h)_\Sigma \end{aligned}$$

for all  $\mathbf{w}_h \in \mathbf{W}_h$ .

- Fluid sub-step: find  $(\mathbf{u}_h^{n,k}, p_h^{n,k}) \in \mathbf{V}_h \times Q_h$  such that

$$\begin{aligned} \rho^f(\partial_\tau \mathbf{u}_h^{n,k}, \mathbf{v}_h)_{\Omega^f} + a_h^f((\mathbf{u}_h^{n,k}, p_h^{n,k}), (\mathbf{v}_h, q_h)) - (\mathbf{u}_h^n - \mathbf{d}_h^{n,k}, q_h \mathbf{n})_\Sigma + \frac{\gamma \mu}{h} (\mathbf{u}_h^{n,k}, \mathbf{v}_h)_\Sigma \\ + \frac{\gamma_0 h}{\gamma \mu} (p_h^{n,k} - p_h^{n,k-1}, q_h)_\Sigma = \frac{\gamma \mu}{h} (\mathbf{d}_h^{n,k}, \mathbf{v}_h)_\Sigma + (\boldsymbol{\sigma}(\mathbf{u}_h^{n,k-1}, p_h^{n,k-1})\mathbf{n}, \mathbf{v}_h)_\Sigma \end{aligned}$$

for all  $(\mathbf{v}_h, q_h) \in \mathbf{V}_h \times Q_h$ .

3. Solution update:

$$\mathbf{u}_h^n = \mathbf{u}_h^{n,K+1}, \quad p_h^n = p_h^{n,K+1}, \quad \mathbf{d}_h^n = \mathbf{d}_h^{n,K+1}, \quad \mathbf{d}_h^n = \mathbf{d}_h^{n,K+1}.$$


---

The next results guarantees the conditional stability of Algorithm 2.

**Lemma 7** Let  $\{(\mathbf{u}_h^n, p_h^n, \mathbf{d}_h^n, \mathbf{d}_h^n)\}_{n \geq 1}$  be the sequence given by Algorithm 2. Then, under the following conditions,

$$C_T^2 \lesssim \gamma, \quad \gamma \tau \lesssim h, \quad 1 \lesssim \gamma_0,$$

$$E^n \lesssim E^0 + \mu \|\mathbf{u}_h^0\|_{0,\Sigma}^2 + \mu \|\boldsymbol{\epsilon}(\mathbf{u}_h^0)\|_{0,\Omega^f}^2 + \frac{\gamma_0 h}{\gamma \mu} \tau \|p_h^0\|_{0,\Sigma}^2$$

for  $n \geq 1$ .

**Proof.** The result follows by combining Lemma 2 with the arguments reported in [6, Section 5.1].

□

The main drawback of Algorithm 2 is its poor accuracy, with respect to Algorithm 1. In fact, the interface time splitting introduces a truncation error whose leading contribution is of the form  $\mathcal{O}(\tau/h)$ , which prevents convergence under the stability conditions of Lemma 7. This error perturbation comes from explicit treatment of the penalty term in the right-hand side of (29). In order to retain overall first-order accuracy under the standard condition  $\tau = \mathcal{O}(h)$  imposed by the stability, we propose to combine Algorithm 2 with an extrapolation/correction strategy (see [7, Section 4.1]).

The resulting procedure is detailed in Algorithm 3, where  $K \geq 0$  indicates the number of correction steps. Here, we have use the notation  $\partial_\tau x^{n,k} = (x^{n,k} - x^{n-1})/\tau$ . The purpose of the second-order extrapolation, in (31), is to retrieve a truncation error in the penalty term of the form  $\mathcal{O}((\tau^2/h)^{K+1})$ , after  $K$ -correction iterations. Note that without any correction, ( $K = 0$ ), this contribution is  $\mathcal{O}((\tau^2/h))$  and hence an overall  $\mathcal{O}(h)$  is expected under  $\tau = \mathcal{O}(h)$ . Numerical evidence shows, however, that  $K \geq 1$  is required for stability.

## 5 Numerical example

In order to illustrate the accuracy and performance of the proposed schemes, we consider the widespread two-dimensional pressure-wave propagation benchmark (see, e.g., [14]). For the sake of simplicity, instead of the linear elasticity equations, a generalized string model is taken for the structure, hence  $\overline{\Omega^s} = \Sigma$  and the relations (2)-(3) are replaced by

$$\begin{cases} \mathbf{u}|_\Sigma = \dot{\mathbf{d}} & \text{in } \Sigma, \\ \rho^s \epsilon \partial_t \dot{\mathbf{d}} + \mathbf{L}^e \mathbf{d} = -\boldsymbol{\sigma}(\mathbf{u}, p) \mathbf{n} & \text{in } \Sigma, \\ \dot{\mathbf{d}} = \partial_t \mathbf{d} & \text{in } \Sigma, \\ \mathbf{d} = \mathbf{0} & \text{on } \partial\Sigma, \end{cases}$$

where

$$\mathbf{d} = \begin{pmatrix} 0 \\ \eta \end{pmatrix}, \quad \mathbf{L}^e \mathbf{d} = \begin{pmatrix} 0 \\ -\lambda_1 \partial_{xx} \eta + \lambda_0 \eta \end{pmatrix}, \quad \lambda_1 \stackrel{\text{def}}{=} \frac{E\epsilon}{2(1+\nu)}, \quad \lambda_0 \stackrel{\text{def}}{=} \frac{E\epsilon}{R^2(1-\nu^2)}.$$

As usual, here  $\epsilon$  denotes the thickness,  $E$  the Young modulus and  $\nu$  the Poisson ratio of the solid. All the quantities will be given in the CGS system. The fluid domain and the fluid-solid interface are, respectively,  $\Omega^f = (0, L) \times (0, R)$ ,  $\Sigma = [0, L] \times \{R\}$ , with  $L = 6$  and  $R = 0.5$ . At  $x = 0$  we impose a sinusoidal pressure of maximal amplitude  $2 \times 10^4$  during  $5 \cdot 10^{-3}$  seconds, corresponding to half a period. Zero pressure is enforced at  $x = 6$  and a symmetry condition is applied on the lower wall  $y = 0$ . The solid is clamped at its extremities,  $x = 0, L$ . The fluid physical parameters are given by  $\rho^f = 1.0$ ,  $\mu = 0.035$ , while for the solid we have  $\rho^s = 1.1$ ,  $\epsilon = 0.1$ ,  $E = 0.75 \times 10^6$  and  $\nu = 0.5$ .

Figure 2 shows an example of unfitted and fitted fluid computational meshes considered in the computations. In the unfitted case, we have  $\Omega_{\mathcal{T}^\tau} = [0, 6] \times [0, 0.8]$  and hence  $\overline{\Omega^f} \subset \Omega_{\mathcal{T}^\tau}$ . The ghost-penalty stabilization bi-linear forms in (9) has been defined on the whole computational domain, that is,

$$g_h(\mathbf{u}_h, \mathbf{v}_h) \stackrel{\text{def}}{=} \gamma_g \sum_{K \in \mathcal{T}_h^f} \int_{\partial K} \mu h [\nabla \mathbf{u}_h]_{\partial K} \cdot [\nabla \mathbf{v}_h]_{\partial K},$$

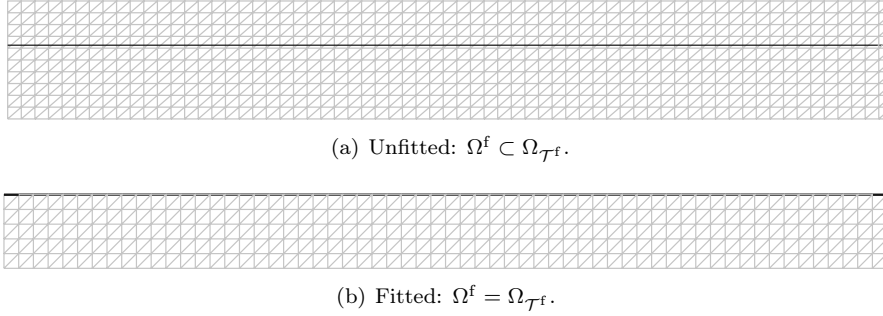


Figure 2: Computational fluid mesh (in grey) and solid domain (in black).

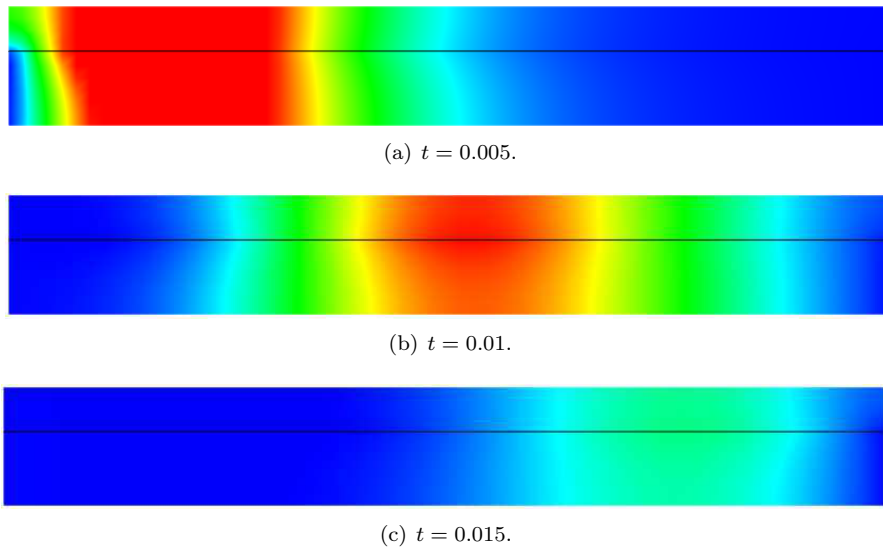


Figure 3: Snapshots of the fluid pressure at different time instants obtained with Algorithm 1.

where the symbol  $[[\cdot]]_F$  denotes the jump of given quantity across the edge or face  $F$ . The free stabilization parameters have been set to  $\gamma_p = 10^{-3}$  and  $\gamma_g = 0.5$ . All the computations have been performed with FreeFem++ [22].

In Figure 3 we have reported a few snapshots of the pressure field obtained with Algorithm 1, taking  $\tau = 2 \cdot 10^{-4}$  and  $h = 0.1$ . The numerical solution remains stable, as predicted by Lemma 6, and a propagating pressure-wave is observed. For comparison purposes, Figure 4 reports the snapshots of the pressure obtained with a fitted method and interface matching discretizations. The good agreement of the two numerical solutions in the physical domain  $\Omega^f$  is clearly visible. Similar conclusions can be inferred from Figure 5, which reports the the corresponding interface displacements at  $t = 0.015$ . The depicted reference solution has been generated using the fitted method with a high space-time grid resolution ( $h = 3.125 \times 10^{-3}$ ,  $\tau = 10^{-6}$ ).

In order to highlight the overall accuracy of Algorithm 1, we have refined both in time and in space at the same rate,  $\tau = \mathcal{O}(h)$ , with the following set of discrete parameters:

$$(\tau, h) \in \{2^{-i} (2 \cdot 10^{-4}, 0.1)\}_{i=0}^4. \quad (32)$$

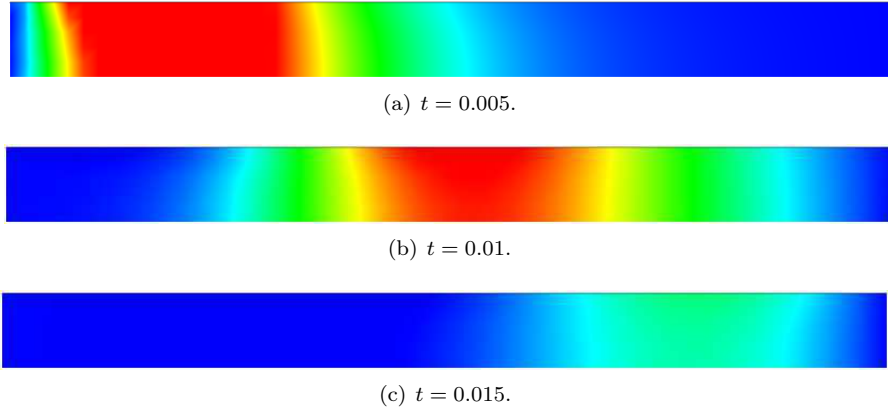


Figure 4: Snapshots of the fluid pressure at different time instants obtained with the fitted method.

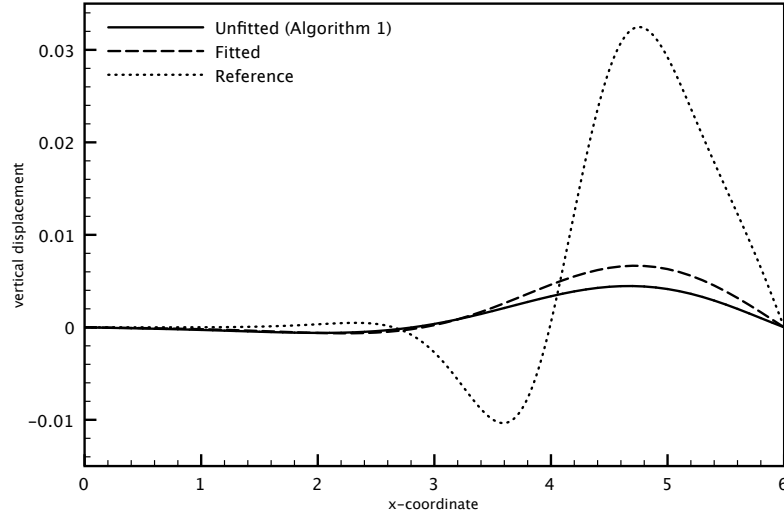


Figure 5: Comparison of the solid displacements at  $t = 0.015$  obtained with  $\tau = 2 \cdot 10^{-4}$  and  $h = 0.1$ .

The coarsest discretization,  $i = 0$ , corresponds to the results reported in Figures 3 and 5. In Figure 6, we have displayed the interface displacements obtained after successive space-time refinement,  $i = 1, \dots, 4$ . These results highlight the convergent behavior of Algorithm 1 and that, after a few space-time refinements, both the fitted and the unfitted methods yields practically the same accuracy.

Figure 7 reports the convergence history of the solid displacement at time  $t = 0.015$ , in the relative elastic energy-norm. The results show that Algorithm 1 retrieves the overall optimal  $\mathcal{O}(h)$  accuracy of the fitted method. Note that, owing to Theorem 5, the accuracy of Algorithm 1 is expected to be  $\mathcal{O}(\tau) + \mathcal{O}(h)$  in the energy norm. Hence, under  $\tau = \mathcal{O}(h)$  we retrieve the optimal  $\mathcal{O}(h)$  rate observed in Figure 7.

We discuss now the explicit coupling procedures introduced in Section 4.2. These methods allow an uncoupled time-marching of the fluid and the solid sub-problems. Figure 8 shows

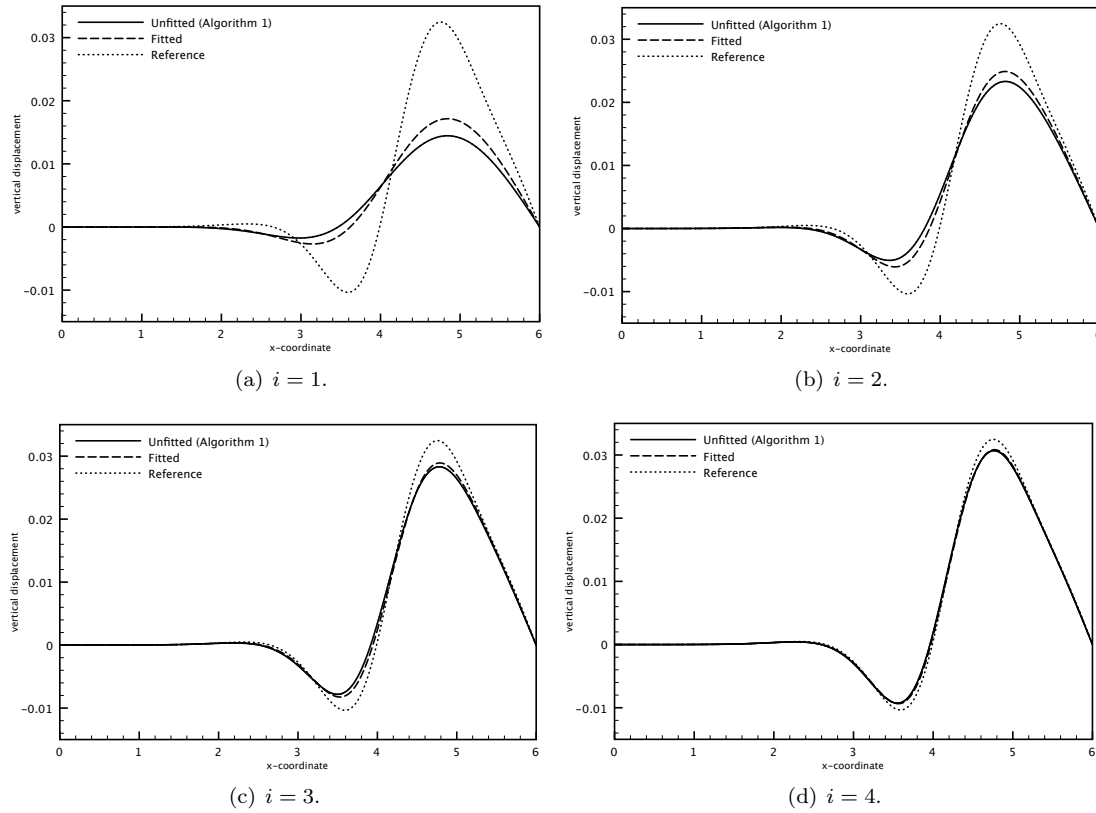


Figure 6: Unfitted vs. fitted methods. Comparison of the solid displacements at  $t = 0.015$  for different levels of  $(\tau, h)$ -refinement, given by (32) with  $i = 1, \dots, 4$ .

the convergence histories of the solid displacement at time  $t = 0.015$ , in the relative elastic energy-norm, obtained with Algorithm 1, Algorithm 2 and Algorithm 3 with  $K = 1$ . The non-convergent behavior of Algorithm 2 under  $\tau = \mathcal{O}(h)$  is striking, as anticipated in Section 4.2. On the contrary, Algorithm 3 with one correction step retrieves the overall optimal  $\mathcal{O}(h)$  accuracy of the implicit coupling scheme (Algorithm 1). Similar observations can be inferred from (9), where we have reported the interface displacements obtained with the last four space-time refinements ( $i = 2, \dots, 5$  in (32)).

## 6 Conclusion

We have introduced a Nitsche's based method for incompressible fluid-structure interaction problems with unfitted meshes. The interface is defined as a part of the solid mesh, which is then glued into the unfitted fluid mesh. The basic ingredients of the method are:

- integration of the fluid equations only in the physical domain (cut-elements);
- Nitsche's treatment of the interface coupling conditions (kinematic/kinetic coupling);
- ghost-penalty stabilization to guarantee robustness.

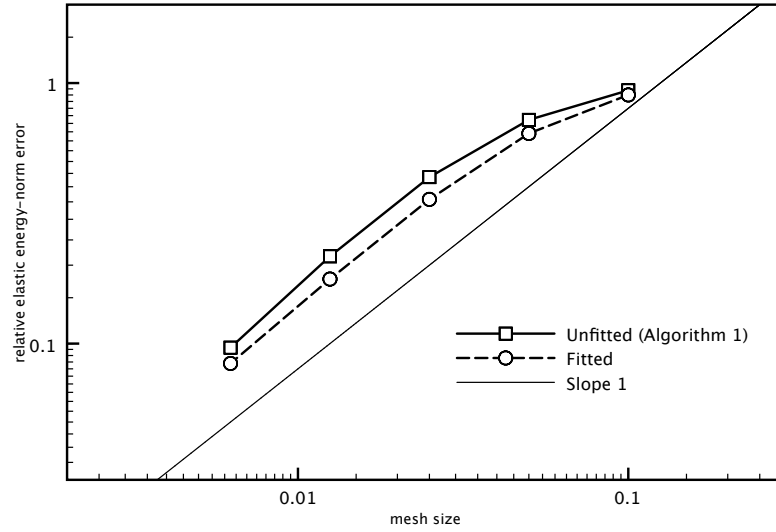


Figure 7: Unfitted vs. fitted methods. Convergence history of the displacement at time  $t = 0.015$ . Space-time grid refinement under  $\tau = \mathcal{O}(h)$ .

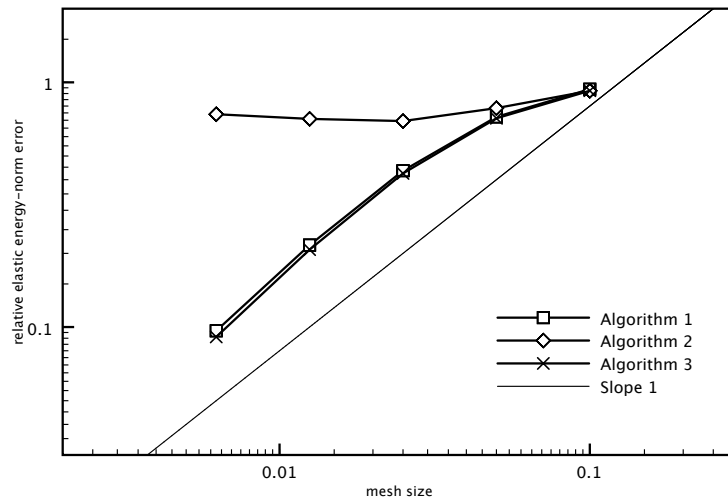


Figure 8: Implicit vs. explicit coupling. Convergence history of the displacement at time  $t = 0.015$ . Space-time grid refinement under  $\tau = \mathcal{O}(h)$ .

For the space semi-discrete formulation, an a priori error estimate has been derived (Theorem 5), which guarantees optimal first-order accuracy. We have then discussed the stability and accuracy of fully discrete formulations based on implicit and explicit coupling schemes. The numerical results confirmed the theoretical findings. In particular, an overall optimal first-order convergent rate was obtained with the implicit schemes (Algorithm 1) and the explicit coupling scheme with extrapolation/correction (Algorithm 1).

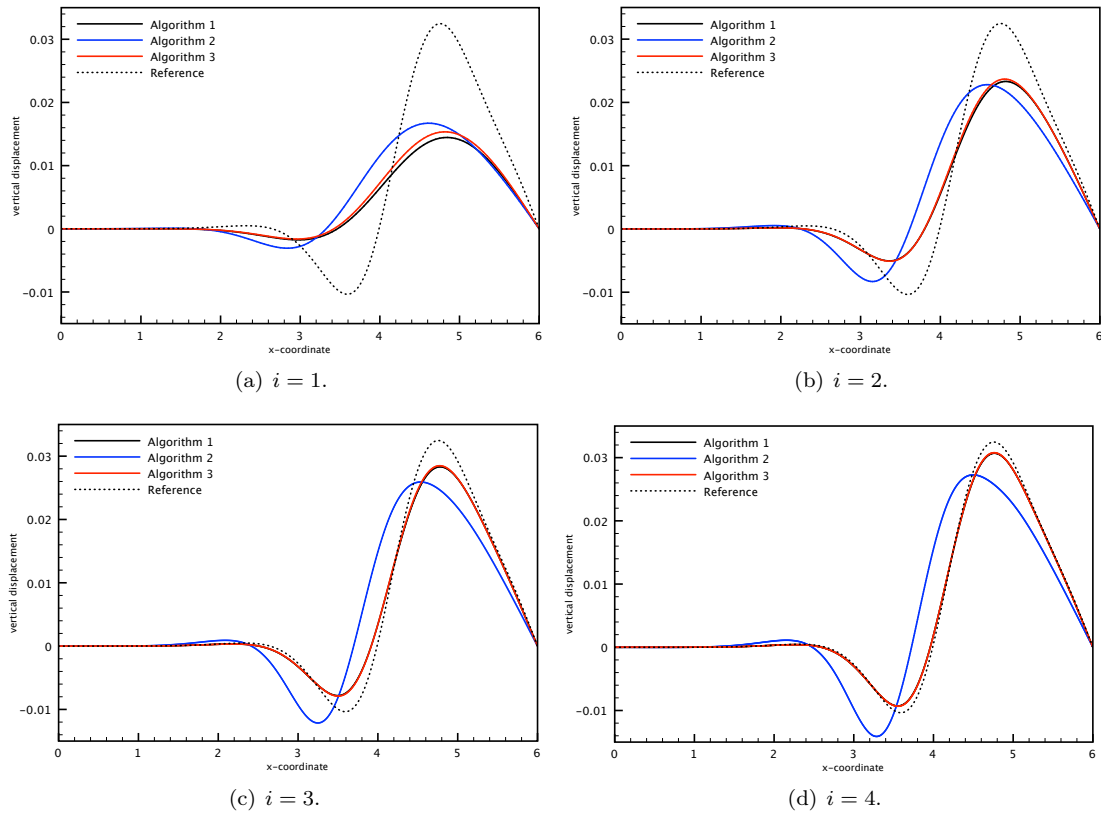


Figure 9: Implicit vs. explicit coupling. Comparison of the solid displacements at  $t = 0.015$  for different levels of  $(\tau, h)$ -refinement, given by (32) with  $i = 1, \dots, 4$ .

Further extensions of this work can explore various directions. An important setting, not covered by the present analysis, is the case of moving interfaces. From the computational point of view, we plan also to address the case of the coupling with non-linear fluid and solid models, and the extension to three-dimensional problems.

## References

- [1] Frank P. T. Baaijens. A fictitious domain/mortar element method for fluid-structure interaction. *Internat. J. Numer. Methods Fluids*, 35(7):743–761, 2001.
- [2] R. Becker, E. Burman, and P. Hansbo. A Nitsche extended finite element method for incompressible elasticity with discontinuous modulus of elasticity. *Comput. Methods Appl. Mech. Engrg.*, 198(41-44):3352–3360, 2009.
- [3] Daniele Boffi, Lucia Gastaldi, Luca Heltai, and Charles S. Peskin. On the hyper-elastic formulation of the immersed boundary method. *Comput. Methods Appl. Mech. Engrg.*, 197(25-28):2210–2231, 2008.

- [4] F. Brezzi and J. Pitkäranta. On the stabilization of finite element approximations of the Stokes equations. In *Efficient solutions of elliptic systems (Kiel, 1984)*, volume 10 of *Notes Numer. Fluid Mech.*, pages 11–19. Friedr. Vieweg, Braunschweig, 1984.
- [5] E. Burman. Ghost penalty. *C. R. Math. Acad. Sci. Paris*, 348(21-22):1217–1220, 2010.
- [6] E. Burman and M.A. Fernández. Stabilization of explicit coupling in fluid-structure interaction involving fluid incompressibility. *Comput. Methods Appl. Mech. Engrg.*, 198(5-8):766–784, 2009.
- [7] E. Burman and M.A. Fernández. Explicit strategies for incompressible fluid-structure interaction problems: Nitsche type mortaring versus Robin-Robin coupling. *Int. J. Num. Meth. Engrg.*, 2013. (2013) In press.
- [8] E. Burman and P. Hansbo. Fictitious domain methods using cut elements: III. a stabilized Nitsche method for Stokes’ problem. Technical report, Jönköping University, 2011. JTH research report, ISSN 1404-0018; 2011:06.
- [9] E. Burman and P. Hansbo. Fictitious domain finite element methods using cut elements: II. A stabilized Nitsche method. *Appl. Numer. Math.*, 62(4):328–341, 2012.
- [10] P. Causin, J.-F. Gerbeau, and F. Nobile. Added-mass effect in the design of partitioned algorithms for fluid-structure problems. *Comput. Methods Appl. Mech. Engrg.*, 194(42–44):4506–4527, 2005.
- [11] N. Diniz dos Santos, J.-F. Gerbeau, and J.-F. Bourgat. A partitioned fluid-structure algorithm for elastic thin valves with contact. *Comput. Methods Appl. Mech. Engrg.*, 197(19-20):1750–1761, 2008.
- [12] Q. Du, M. D. Gunzburger, L. S. Hou, and J. Lee. Analysis of a linear fluid-structure interaction problem. *Discrete Contin. Dyn. Syst.*, 9(3):633–650, 2003.
- [13] M.A. Fernández. Coupling schemes for incompressible fluid-structure interaction: implicit, semi-implicit and explicit. *SĕMA J.*, (55):59–108, 2011.
- [14] L. Formaggia, A. Quarteroni, and A. Veneziani, editors. *Cardiovascular Mathematics. Modeling and simulation of the circulatory system*, volume 1 of *Modeling, Simulation and Applications*. Springer, 2009.
- [15] Axel Gerstenberger and Wolfgang A. Wall. An extended finite element method/Lagrange multiplier based approach for fluid-structure interaction. *Comput. Methods Appl. Mech. Engrg.*, 197(19-20):1699–1714, 2008.
- [16] R. Glowinski, T.-W. Pan, T.I. Hesla, and D.D. Joseph. A distributed lagrange multiplier/fictitious domain method for particulate flows. *Int. J. Multiphase Flow*, 25(5):755–794, 1999.
- [17] A. Hansbo and P. Hansbo. An unfitted finite element method, based on Nitsche’s method, for elliptic interface problems. *Comput. Methods Appl. Mech. Engrg.*, 191(47-48):5537–5552, 2002.
- [18] A. Hansbo and P. Hansbo. A finite element method for the simulation of strong and weak discontinuities in solid mechanics. *Comput. Methods Appl. Mech. Engrg.*, 193(33-35):3523–3540, 2004.

- 
- [19] A. Hansbo, P. Hansbo, and M. G. Larson. A finite element method on composite grids based on Nitsche's method. *M2AN Math. Model. Numer. Anal.*, 37(3):495–514, 2003.
- [20] P. Hansbo. Nitsche's method for interface problems in computational mechanics. *GAMM-Mitt.*, 28(2):183–206, 2005.
- [21] P. Hansbo, J. Hermansson, and T. Svedberg. Nitsche's method combined with space-time finite elements for ALE fluid-structure interaction problems. *Comput. Methods Appl. Mech. Engrg.*, 193(39-41):4195–4206, 2004.
- [22] F. Hecht. New development in FreeFem++. *J. Numer. Math.*, 20(3-4):251–265, 2012.
- [23] P. Le Tallec and S. Mani. Numerical analysis of a linearised fluid-structure interaction problem. *Numer. Math.*, 87(2):317–354, 2000.
- [24] A. Legay, J. Chessa, and T. Belytschko. An Eulerian-Lagrangian method for fluid-structure interaction based on level sets. *Comput. Methods Appl. Mech. Engrg.*, 195(17-18):2070–2087, 2006.
- [25] A. Massing, M. Larson, A. Logg, and M. Rognes. A stabilized nitsche overlapping mesh method for the stokes problem. Technical report, 2012. arXiv:1205.6317.

## Contents

<b>1</b>	<b>Introduction</b>	<b>3</b>
<b>2</b>	<b>A linear model problem</b>	<b>4</b>
<b>3</b>	<b>Space semi-discretization: Nitsche fictitious domain formulation</b>	<b>5</b>
3.1	Stability properties of the discrete scheme. . . . .	7
3.2	Consistency of the formulation . . . . .	7
3.3	Error analysis . . . . .	8
<b>4</b>	<b>Time discretization: coupling schemes</b>	<b>13</b>
4.1	Implicit coupling . . . . .	13
4.2	Explicit coupling . . . . .	14
<b>5</b>	<b>Numerical example</b>	<b>16</b>
<b>6</b>	<b>Conclusion</b>	<b>19</b>



**RESEARCH CENTRE  
PARIS – ROCQUENCOURT**

Domaine de Voluceau, - Rocquencourt  
B.P. 105 - 78153 Le Chesnay Cedex

Publisher  
Inria  
Domaine de Voluceau - Rocquencourt  
BP 105 - 78153 Le Chesnay Cedex  
[inria.fr](http://inria.fr)

ISSN 0249-6399